Temperature Dependence of Thin Film Spiral Inductors on Alumina over a Temperature Range of 25 to 475º C

George E. Ponchak, Jennifer L. Jordan and Maximilian C Scardelletti
NASA Glenn Research Center
21000 Brookpark Rd
Cleveland, OH 44135
george.ponchak@ieee.org

Abstract

In this paper, we present an analysis of inductors on an Alumina substrate over the temperature range of 25 to 475º C. Five sets of inductors, each set consisting of a 1.5, 2.5, 3.5, and a 4.5 turn inductor with different line width and spacing, were measured on a high temperature probe station from 10 MHz to 30 GHz. From these measured characteristics, it is shown that the inductance is nearly independent of temperature for low frequencies compared to the self resonant frequency, the parasitic capacitances are independent of temperature, and the resistance varies nearly linearly with temperature. These characteristics result in the self resonant frequency decreasing by only a few percent as the temperature is increased from 25 to 475º C, but the maximum quality factor decreases by a factor of 2 to 3. These observations based on measured data are confirmed through 2D simulations using Sonnet software.

I. Introduction

High temperature electronic circuits are finding many uses for a variety of commercial applications. For example, a variety of high temperature sensors are required for automobiles, including on-engine sensors that operate up to 150º C, power brake sensors that operate through 140º C, and engine exhaust sensors operating through 850º C [1]. The development of geothermal energy is progressing rapidly because it is a clean energy, but the drilling to and monitoring of the subterranean temperature requires sensors operating to as high as 300º C [2]. The oil and natural gas drilling industry requires sensors and electronics that operate through 225º C [3]. Aircraft engine intelligent control and health monitoring require many different sensors [4] that operate over a range of temperatures through 500º C [5], [6], and probably higher.

Many high temperature electronic circuits and sensors rely on inductors. Some RFID tags use a tuned LC circuit in which the capacitance varies with an environmental variable and the resulting change in the resonant frequency is detected [7], [8]. High temperature oscillators operating at 200º C and 270º C [9], [10] and wireless sensors operating at 400º C [11], [12] use an LC tuned oscillator to frequency modulate a signal that varies with an environmental variable. Thus, it is critical to understand how the inductor behaves as a function of temperature.

Several papers have been published with limited measured characteristics of thin film inductors as a function of temperature. Inductors have been characterized on high resistivity silicon and sapphire substrates over a temperature range of 25 to 150º C [1], on a BiCMOS silicon substrate over a temperature range of 25 to 125º C [2], and on a CMOS silicon substrate over a temperature range of 25 to 100º C [3]. On a GaAs substrate with a polyimide interface layer, inductors were characterized over the temperature range of 25 to 185º C [4]. Unfortunately, Si and GaAs are not suitable substrates for high temperature circuits. A preliminary set of measurements of inductors on a SiC substrate, which is capable of supporting high temperature circuits, over a temperature range of 25 to 200º C was presented in [5].

In this paper, five sets of inductors with different numbers of turns, different inner radius, and different line widths are measured as a function of temperature. From the measured, results, conclusions are derived. These are confirmed with EM simulations of the inductors. Section II describes the inductors, Section III describes the measurement procedures, Section IV presents the measured results, and Section V discusses the results.

II. Description of Inductors

Figure 1 shows a line drawing of an inductor from the mask file. The dimension of the inner rectangle is called R, the width of the metal traces in the inductor is W, and the space between the coils is S. As seen in Fig. 1, the inductor has a ground connection between the two RF probe ports on the left and right hand sides. The distance between the coil and the ground is kept at 200 μm in all of the test structures. Table I shows all of the other the dimensions.

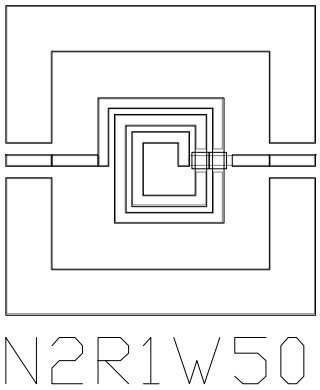

Figure 1: Line drawing of inductor mask.

Table I: Dimensions of 5 sets of inductors.

# Turns	W (μm)	S (μm)	R (μm)
1.5, 2.5, 3.5, 4.5	50	25	150
1.5, 2.5, 3.5, 4.5	75	25	150
1.5, 2.5, 3.5, 4.5	25	25	150
1.5, 2.5, 3.5, 4.5	50	25	250
1.5, 2.5, 3.5, 4.5	25	25	250

The inductors were fabricated on a 508 μm thick, 99.6 %, double side polished alumina substrate. The metal structures were defined through a "lift-off" process with a 0.025 μm thick Ti adhesion layer, a 0.51 μm thick first level Au layer, and a 1.0 μm thick second level Au layer. The entire coil is therefore 1.51 μm thick except under the crossover, which is 0.51 μm. Because the inductors are being characterized at temperatures through 475º C, an airbridge is not used. Instead, the crossover is supported by a SiO_2/Si_3N_4 stack that is 0.85 μm thick.

III. Measurement and Modeling Procedures

The inductors were characterized on a high temperature RF probe station [18]. In two sets of measurements, GGB Industries, Model 50A RF probes modified by the manufacturer for high temperature testing were used for measurements from 25 to 475º C [18]. For this set of measurements, on-wafer short/open/load/thru (SOLT) calibration was performed at each temperature through 175º C with the GGB Industries cal standard wafer; for higher temperatures, the 175º C calibration was used. In a third set of measurements, Suss MicroTec |Z| probes were used from 25 to 325º C, with the SUSS SOLT calibration standard used to calibrate at every temperature through 225º C; again, for temperatures higher than 225º C, the 225º C calibration was used. After the SOLT calibration, which establishes the reference plane at the probe tips, an open and a short circuit structure as shown in Fig. 2 was measured for pad removal using the Cascade WinCal software. The pad removal corrects for the capacitance and inductance caused by the pads, and it is therefore expected to correct for small variations in the probe parasitic reactance due to a change in temperature for the higher temperatures where the wafer calibration was not performed.

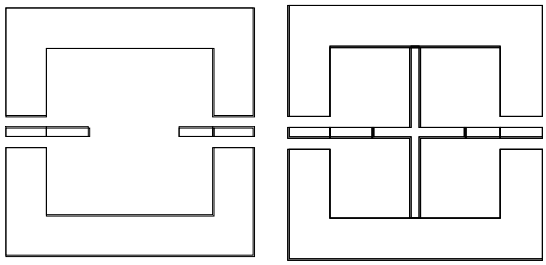

Figure 2: Open and short structures for pad parasitic reactance removal.

The measured S-parameters were analyzed by two methods. First, the S-parameters were used in ADS Software and fit to the equivalent circuit shown in Fig. 3. For the fitting, the measured data through the Self Resonant Frequency (SRF) was used, and the gradient optimization routine was performed. Note that this method results in frequency independent component values.

In the second method, the S-parameters were converted to Y-parameters. Then, the equivalent model shown in Fig. 4 (Note that the capacitance C_P cannot be separated from the inductance in the series arm) was used to determine the equivalent circuit element values by:

$$\omega C1=\mathrm{Im}(Y_{11}+Y_{12}) \quad (1)$$

$$\omega C2=\mathrm{Im}(Y_{22}+Y_{12}) \quad (2)$$

$$R=-Re(1/Y_{12}) \quad (3)$$

$$\omega L=-Im(1/Y_{12}) \quad (4)$$

where ω is the frequency in radians, *Re(X)* is the real part of *X*, and *Im(X)* is the imaginary part of *X*. Note that this method yields frequency dependant parameters. Thus, for determining the inductance and resistance, the average inductance or resistance from 0.5 to 2 GHz where the parameter variation with frequency is small (See next section) was used. Because capacitance is difficult to determine at low frequency, the average capacitance from 1.5 to 4 GHz was used. The quality factor, Q, is found from

$$Q=\omega L/R=-Im(Y_{11})/Re(Y_{11}) \quad (5)$$

and the SRF is determined from where Q=0, which is the same as L=0.

2D electromagnetic simulations of 1.5 and 4.5 turn inductors were performed with Sonnet software. Both inductors were simulated at 25, 175, 325 and 475º C; to account for the rise in temperature, only the metal resistivity was varied according to $\rho=\rho_o(1+\alpha\Delta T)$, where $\rho_o=2.44$ μΩ·cm at 20º C, $\alpha=0.0034$/º C, and ΔT is the temperature difference from 20º C [19]. The pad removal structures were also simulated in Sonnet, and the resulting S-parameter files for the inductors and the pad calibration structures were used in WinCal to obtain calibrated S-parameter files of the inductors. These were then converted to Y-parameters and the equivalent circuit component values were determined.

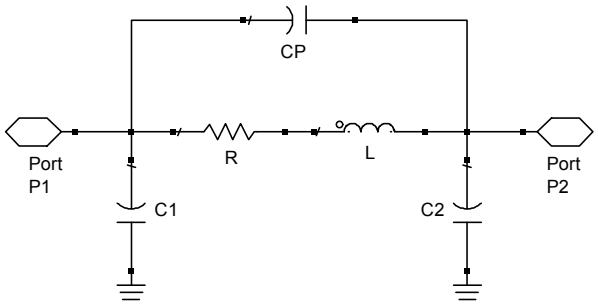

Figure 3: Equivalent circuit model of inductor for ADS model extraction.

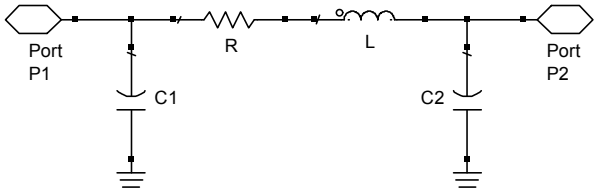

Figure 4: Equivalent circuit model for Y-parameter model extraction.

IV. Measured Results

To provide a sample of the data and to give a qualitative understanding of the data, the measured equivalent circuit parameters for Fig. 4, calculated from the Y-parameters for the 1.5 turn inductor of the first row of Table I, are shown in Figs. 5-7, and Fig. 8 shows the resulting quality factor. It is seen that the inductance has the typical relationship with frequency; it is nearly constant at low frequency and increases

dramatically as the self resonant frequency is approached. The range of inductances characterized in this paper is 0.8 to 18 nH. The capacitances C1 and C2 are nearly independent of frequency, and R increases with frequency as expected due to the frequency dependence of the skin depth [20]. It is also seen that L, C1, and C2 are nearly independent of temperature, while R increases with temperature as expected due to the increase in resistivity with temperature. Because to a first order $Q=\omega L/R$, the maximum Q decreases with temperature.

The equivalent circuit parameters for each inductor were also determined by ADS. Figs. 9-11 show the ADS and the Y-parameters inductance, capacitances C1 and C2, and resistance, R, respectively, determined for the 1.5 turn inductor of row 1 of Table I as a function of temperature. It is seen that the inductance determined by the two methods agrees well, with the Y-parameter inductance being higher; this is expected because the Y-parameter inductance incorporates the capacitance C_P, which, to a first order, increases the inductance by a factor of $1/(1-\omega^2 LC_P)$. C1, C2, and R also agree well between the two methods. Because of the good agreement between the two methods, both or either can be used throughout the paper to determine the temperature dependence of the inductor parameters. Also plotted on Figs. 9-11 is the equivalent circuit parameters calculated from the Sonnet simulations; it is seen that these also agree well with the measured data.

So far, data for only a single inductor has been shown. To draw more complete conclusions, Figs. 12-14 show the normalized variation of L, self resonant frequency (SRF), and Q_{max} as a function of temperature for every inductor measured and the Sonnet simulations ($\Delta L=[L(T)-L(25^\circ C)]/L(25^\circ C)$. The definitions for SRF and Q_{max} are similar). In Fig. 12, it is seen that the variation or error in the measured inductances is less than 10%; the data also shows that L increases by less than 2% as the temperature increases from 25 to 500º C. The inductance derived from the EM simulations agrees with the measured data. In Fig. 13, the measured SRF shows a decrease of 2% while the Sonnet simulations show a 0% change as the temperature increases from 25 to 500º C. The variation of Q_{max} with temperature is substantial, with an average decrease in Q_{max} of 60% over the temperature range of 25 to 500º C.

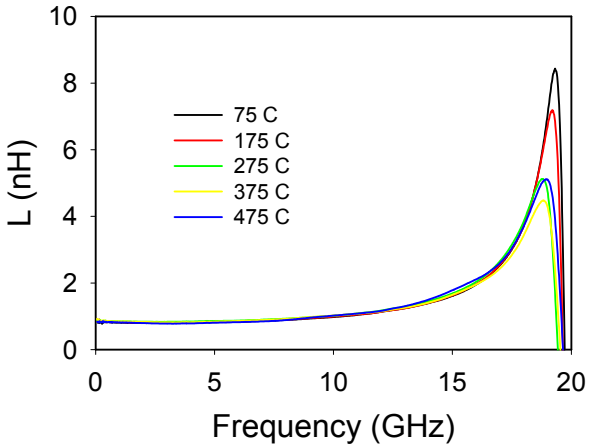

Figure 5: Inductance as a function of frequency and temperature for 1.5 turn inductor from row 1 of Table I.

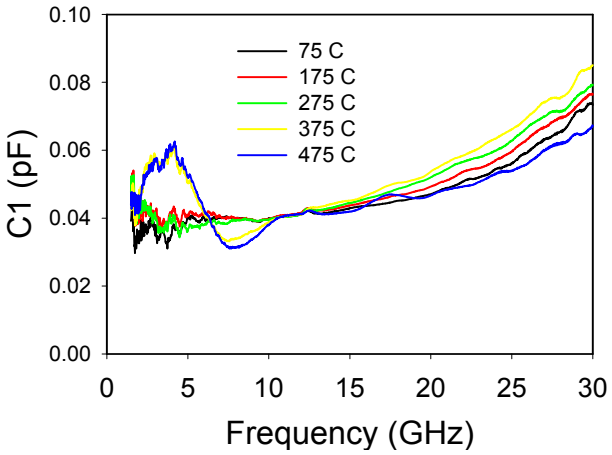

(a)

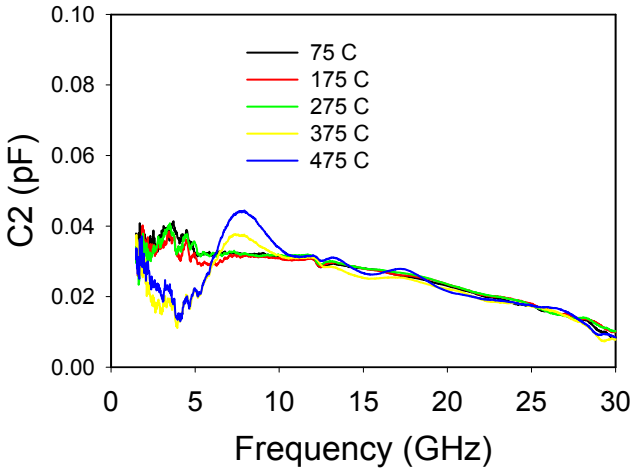

(b)

Figure 6: C1 and C2 as a function of frequency and temperature for 1.5 turn inductor from row 1 of Table I.

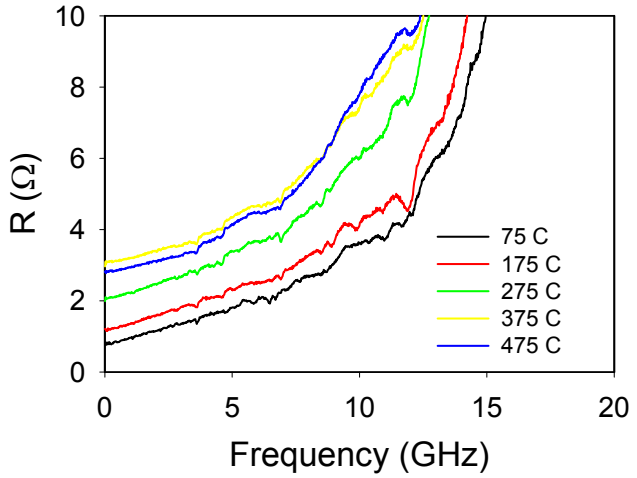

Figure 7: R as a function of frequency and temperature for 1.5 turn inductor from row 1 of Table I.

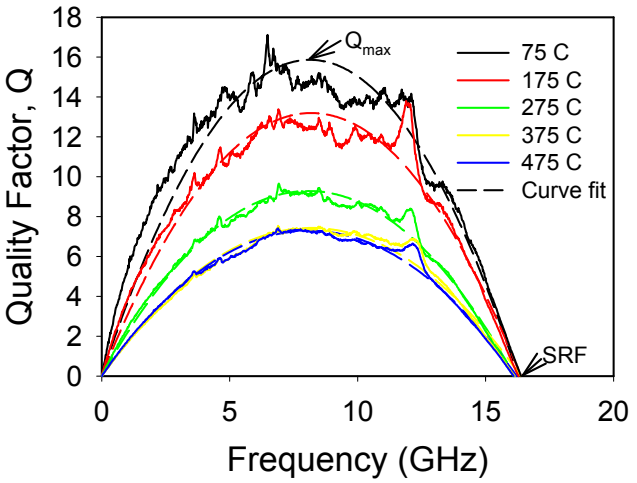

Figure 8: Q as a function of frequency and temperature for 1.5 turn inductor from row 1 of Table I.

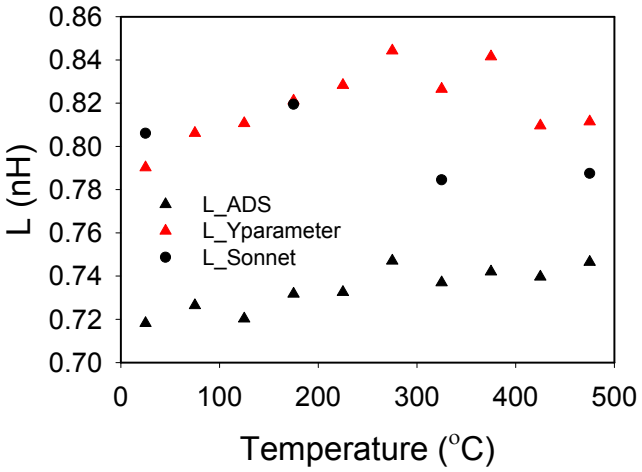

Figure 9: L as a function of temperature for the 1.5 turn inductor of row 1 of Table I determined by ADS, the Y-parameters, and Sonnet.

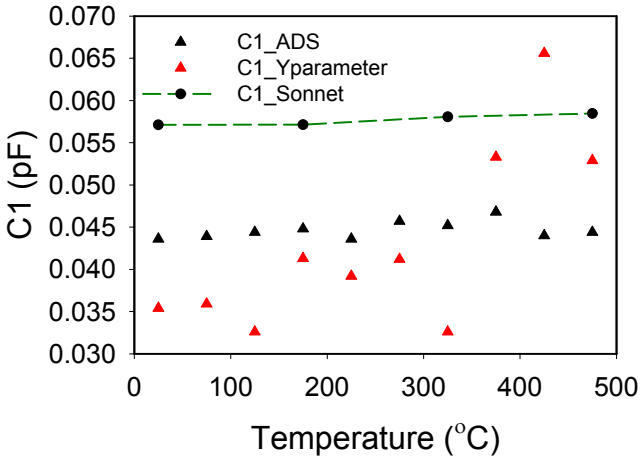

(a)

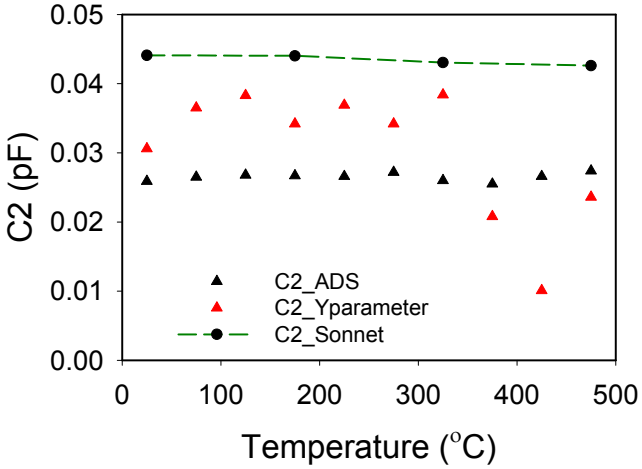

(b)

Figure 10: C1 and C2 as a function of temperature for the 1.5 turn inductor of row 1 of Table I determined by ADS, the Y-parameters, and Sonnet.

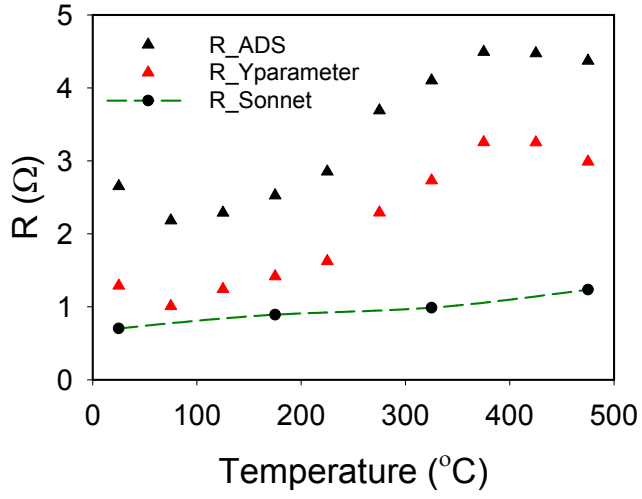

Figure 11: R as a function of temperature for the 1.5 turn inductor of row 1 of Table I determined by ADS, the Y-parameters, and Sonnet.

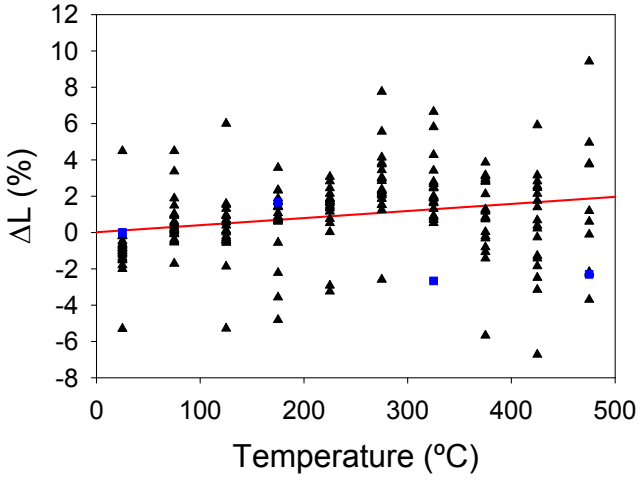

Figure 12: Normalized change in inductance as a function of temperature for all inductors measured. Blue squares are the same for Sonnet simulations.

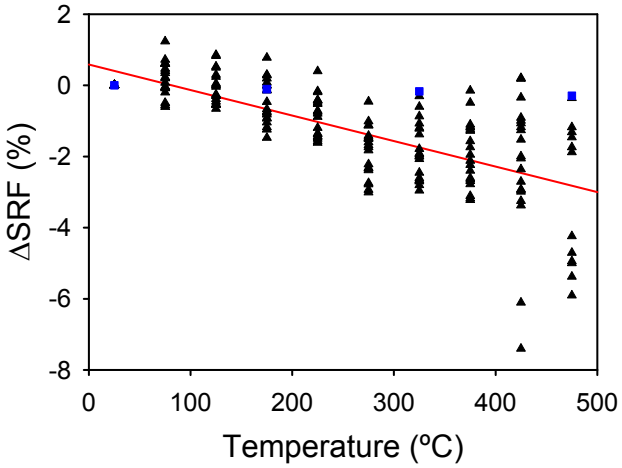

Figure 13: Normalized change in self resonant frequency as a function of temperature for all inductors measured. Blue squares are the same for Sonnet simulations.

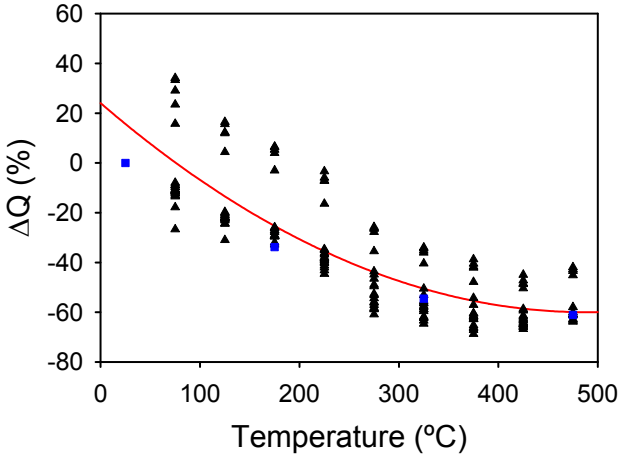

Figure 14: Normalized change in Q_{max} as a function of temperature for all inductors measured. Blue squares are the same for Sonnet simulations.

V. Discussions

The inductance of a metal strip or an inductor is comprised of internal inductance, self inductance and mutual-inductance. The self and mutual inductances are dependent on the permeability of the surrounding material and the physical layout of the inductor, such as W, S, R, and the number of turns [21], [22]. Since none of these parameters vary appreciably with temperature, the self and mutual inductances are not expected to vary with temperature. The internal inductance of the metal strip is [23]:

$$L_i = \frac{l}{\omega W}\sqrt{\pi f \mu_0 \rho} = \frac{l}{\omega W}\sqrt{\pi f \mu_0 \rho_0}\ \sqrt{1+\alpha \Delta T} \quad (6)$$

where l is the length of the strip or coil. Thus, L_i varies with temperature as:

$$\frac{\partial L_i}{\partial T} = L_i \frac{\alpha}{2(1+\alpha T)} \quad (7)$$

Since α=0.0034/º C, the maximum expected percentage change in internal inductance is 0.17 %. Since the internal inductance is small compared to the self and the mutual inductance, the expected temperature variation in inductance is expected to be very small. This agrees with the data shown in Fig. 12 and the results of the prior cited papers.

The SRF can be shown to be:

$$SRF = \frac{1}{2\pi\sqrt{LC}}\sqrt{1-\frac{R^2 C}{L}} \quad \text{(Hz)} \quad (8)$$

where $C=C_I+C_P$. Since $R^2C \ll L$ for a typical inductor, the SRF may be approximated as:

$$SRF = \frac{1}{2\pi\sqrt{LC}}\left(1-\frac{R^2 C}{2L}\right) \quad (9)$$

Differentiating SRF with respect to T and again using $R^2C \ll L$ yields:

$$\frac{\partial SRF}{\partial T} = SRF\,\frac{-C}{L}\,\frac{\partial R}{\partial T} \quad (10)$$

Because C<<L and resistance increases with temperature for metals, the percentage change in SRF is expected to be negative and small due to an increase in temperature. This agrees with Fig. 13. Because SRF is nearly constant with temperature and L has been shown to be constant with temperature, it follows that C must also be constant with temperature, as shown in Fig. 10. Also, since the frequency at which Q is maximum, f_{Qmax}, can be shown to be SRF/√3, f_{Qmax} is not expected to vary with temperature either; this is seen in Fig. 8.

The resistance is expected to increase with temperature because the resistivity increases with temperature. The DC resistance of a metal strip is known to be R=ρl/Wt, where all of the parameters have already been defined. At high frequencies, the current does not uniformly flow through the cross section of the strip, and the resistance can be estimated as [20]:

$$R = \frac{l}{W}\sqrt{\pi f \mu_0 \rho}\ \frac{1}{(1-e^{-t/\delta})} \quad (11)$$

where δ is the skin depth. If t/δ>>1 (or f→∞), then

$$R = \frac{l\sqrt{\pi f \mu_0 \rho}}{W} \tag{12}$$

and if t/δ<<1 (or f→0) and using a Taylor series expansion of $1-e^{-t/\delta}$, the usual DC resistance is obtained. Thus, the resistance R(f,T) in the two limits is:

$$R(0,T) = \frac{l\rho_0}{W t}\left[1+\alpha T\right] \tag{13a}$$

$$R(\infty,T) = \frac{l}{W}\sqrt{\pi f \mu_0 \rho_0}\ \sqrt{1+\alpha T} \tag{13b}$$

For αT<<1, or T<200º C, (13b) may be approximated as:

$$R(\infty,T) = \frac{l}{W}\sqrt{\pi f \mu_0 \rho_0}\ \left[1+\frac{\alpha T}{2}\right] \tag{14}$$

Thus, from (13a) and (14), the resistance is expected to increase linearly with temperature. By using a linear regression fit through the resistance versus temperature data and taking the ratio of the slope to the intercept point, according to (13a) and (14), the result should be either α or α/2, respectively. In fact, the ratio is $6.791\cdot10^{-3} \pm 2.4817\cdot10^{-3}$, which is a factor of 2 greater than the handbook value of 0.0034. It is noted that α determined by this method is greater than the handbook value for all of the inductor geometries.

The maximum Q can be derived as:

$$Q_{\max} = \frac{2}{3\sqrt{3}}\sqrt{\frac{L}{C}}\frac{1}{R} \tag{15}$$

where $R^2C<<L$ is again assumed. Since R is the only component that varies with temperature and it is expected to vary as $R(T)=R_0(1+\alpha T)$, where R_0 is the 20º C resistance, Q_{max} is expected to decrease with temperature as $(1+\alpha T)^{-1}$. Using the handbook value of α=0.0034, the expected decrease in Q_{max} as the temperature is increased from 20 to 500º C is 62%. If the value of α found from the linear fit to the measured R is used, Q_{max} should decrease by 77 % over the same temperature range. The ΔQ_{max} shown in Fig. 14 is within the range of these values.

VI. Conclusions

Thus, the inductance and parasitic capacitance of thin film, planar inductors on alumina substrates have been shown to not vary appreciably as a function of temperature, which agrees with the conclusions from previous papers that were based on a smaller range of temperatures. Therefore, the frequency of high temperature oscillators or other resonant circuits is not expected to vary by more than a few percent due to variations in the inductance. However, the resistance does vary, causing the maximum Q to decrease by approximately 70% over the temperature range of 20 to 500º C, and this may affect the inductor's ability to satisfy circuit requirements.

Acknowledgments

The authors wish to acknowledge and thank Nicholas Varaljay and Elizabeth McQuaid for fabricating the test structures and the NASA IVHM program for funding the research.

References

1. R. W. Johnson, J. L. Evans, P. Jacobsen. J. R. Thompson and M. Christopher, "The changing automotitive environment: high-temperature electronics," *IEEE Trans. Electronics Packaging Manufacturing*, Vol. 27, No. 3, pp. 164-176, July 2004.
2. B. A. Goldstein, A. J. Hill, A. Long, A. R. Budd, F. Holgate, and M. Malavazos, "Hot rock geothermal energy plays in Australia," in *Proc. Thirty-Fourth Workshop on Geothermal Reservoir Engineering*, Stanford Univ., Stanford, CA, Feb. 9-11, 2009.
3. R. A. Normann, "First high-temperature electronics products survey 2005," Sandia National Laboratories Sandia Report SAND2006-1580, April 2006.
4. J. S. Litt, D. L. Simon, S. Garg, Ten-Heui Guo, C. Mercer, R. Millar, A. Behbahani, A. Bajwa, and D. T. Jensen, "A survey of intelligent control and health management technologies for aircraft propulsion systems," NASA/TM-2005-213622, ARL-TR-3413, May 2005.
5. A. R. Behbahani, "Need for robust sensors for inherently fail-safe gas turbine engine controls, monitoring, and prognostics," AFRL-PR-WP-TP-2007-217, Nov. 2006, also in Proc. 2006 52nd Int. Instrumentation Symp.
6. D. E. Culley, R. Thomas and J. Saus, "Concepts for distributed engine control," NASA TM 2007-214994, Nov. 2007.
7. Klaus Finkenzeller, *RFID Handbook*, 2nd Edition, John Wiley & Sons, Hoboken, NJ, 2003.
8. D. G. Watters, P. Jayaweera, A. J. Bahr, and D. L. Huestis, "Design and performance of wireless sensors for structural health monitoring," *AIP Conf. Proc. 615: Quantitative Nondestructive Evaluation*, May 2002, pp. 969-976.
9. Z. D. Schwartz and G. E. Ponchak, "1 GHz, 200 ºC, SiC MESFET Clapp oscillator," *IEEE Microwave and Wireless Component Lett.*, Vol. 15, No. 11, pp. 730-732, Nov. 2005.
10. G. E. Ponchak, M. C. Scardelletti and J. L. Jordan, "270° C, 1 GHz oscillator-type active antenna," *IET Electronics Letters*, Vol. 45, Issue 8, April 9, 2009, pp. 386-387.
11. M. Suster, D. J. Young and Wen H. Ko, "Micro-power wireless transmitter for high-temperature MEMS sensing and communication applications," *Proc. IEEE Microelectromechanical Systems (MEMS) 2002*, Las Vegas, NV, Jan. 20-24, 2002, pp. 641-644.
12. Run Wang, Wen H. Ko and D. Young, "silicon-carbide MESFET-based 400 º C MEMS sensing and data telemetry," *IEEE Sensors Journal*, Vol. 5, No. 6, Dec. 2005, pp. 1389-1394.
13. J. N. Burghartz, D. C. Edelstein, K. A. Jenkins, and Y. H. Kwark, "Spiral inductors and transmission lines in silicon technology using copper-damascene interconnects and low-loss substrates," *IEEE Trans. Micro. Theory and Tech.*, Vol. 45, No. 10, pp. 1961-1968, Oct. 1997.

14. R. Groves, D. L. Harame, and D. Jadus, "Temperature dependence of Q and inductance in spiral inductors fabricated in a silicon-germanium/BiCMOS technology," *IEEE Journ. Solid-State Circuits*, Vol. 32, No. 9, pp. 1455-1459, Sept. 1997.
15. Kai Kang, Jinglin Shi, Wen-Yan Yin, Le-Wei Li, S. Zouhdi, S. C. Rustagi, and K. Mouthaan, "Analysis of frequency- and temperature-dependent substrate eddy currents in on-chip spiral inductors using the complex image method," *IEEE trans on Magnetics*, Vol. 43, No. 7, pp. 3243-3253, July 2007.
16. Wen-Yan Yin, Jun-Fa Mao, Jing-Lin Shi and Xiao-Wei Sun, "Performance degradation of some on-chip finite-ground coplanar waveguide (FGCPW)-built passive devices at high temperature," *Micro. And Opt. Tech. Letters*, Vol. 48, No. 9, pp. 1754-1759, Sept. 2006.
17. Z. D. Schwartz, G. E. Ponchak, S. A. Alterovitz, A. N. Downey, and C. T. Chevalier, "Measurement of thin film integrated passive devices on SiC through 500° C," *34th European Microwave Conf. Dig.*, Amsterdam, The Netherlands, Oct. 11-15, 2004, pp. 313-316.
18. Z. D. Schwartz, A. N. Downey, S. A. Alterovitz, and G. E. Ponchak, "High-temperature RF probe station for device characterization through 500 º C and 50 GHz," *IEEE Trans. on Instrumentation*, Vol. 54, No. 1, pp. 369-376, Feb. 2005.
19. *CRC Handbook of Chemistry and Physics*, 62nd Edition, Eds. R. C. Weast and M. J. Astle, CRC Press, Boca Raton, FL, 1981.
20. Min Park, Chung-Hwan Kim, Cheon Soo Kim, Mun-Yang Park, Sung-Do Kim, Young-Sik Youn, and Hyun Kyu Yu, "Frequency-dependent series resistance of monolithic spiral inductors," *IEEE Micro. and Guided Wave Letters*, Vol. 9, No. 12, pp. 514-516, Dec. 1999.
21. J. Crols, P. Kinget, J. Craninckx and M. Steyaert, "An analytical model of planar inductors on lowly doped silicon substrates for high frequency analog design up to 3 GHz," *IEEE Symp. VLSI Circuits Dig.*, 1996, pp. 28-29.
22. S. S. Mohan, M. del Mar Hershenson, S. P. Boyd, and T. H. Lee, "Simple accurate expressions for planar spiral inductances," *IEEE Journal Solid-State Circuits*, Vol. 34, No. 10, pp. 1419-1424, Oct. 1999.